GEOPHYSICAL MODELING IN EURASIA: 2D CRUSTAL P AND LG PROPAGATION; UPPER-MANTLE SHEAR WAVE PROPAGATION AND ANISOTROPY; AND 3D, JOINT, SIMULTANEOUS INVERSIONS

Charlotte A. Rowe, Monica Maceira, Michael L. Begnaud, Lee K. Steck, and W. Scott Phillips

Los Alamos National Laboratory

Sponsored by National Nuclear Security Administration

Contract No. DE-AC52-06NA25396

ABSTRACT

New tomographic models have been developed to obtain improvements to travel-time predictions for a variety of crustal and upper-mantle seismic phases, and we approach the problem with both independent datasets and joint, simultaneous inversion of diverse geophysical parameters.

New Pg and Lg velocity models in Eurasia improve estimates of crustal travel times across the region. Inversion of Pg and Lg travel times improves RMS by ~30% compared to iasp91. Site terms for both phases show similar patterns and likely reflect thicknesses and velocities of sediments above the upper crust. Event terms are ~1 s, suggesting 5–10-km-average depth errors. Velocities are consistent with typical upper-crustal velocities set forth in the Department of Energy (DOE) Unified Model but suggest more geographic variability.

Upper-mantle shear wave (Sn) velocity tomography, including Sn gradient within the upper mantle, has been performed both with and without anisotropy. We use events that are GT25 and better, with depths of <50 km and path lengths between 400 and 1700 km. The 14,645 events recorded at 2,399 stations yielded 144,933 raypaths. Most arrivals were obtained from the International Seismological Centre (ISC), Annual Bulletin of Chinese Earthquakes (ABCE), and Earthquake Data Reports (EDR) catalogs. Crustal leg corrections assume 45-km average crustal thickness, 3.6-km/s velocity, and 52-degree incidence angles beneath station and source. The RMS reduction after inversion is ~56%. Sn velocities mirror those found for Pn; however, the Sn gradient appears to be weaker. Solving for anisotropy removes some high-frequency oscillations; the anisotropy appears to follow that found for Pn.

Motivated by the shortcomings of existing single-parameter inversion methods in accurate prediction of both seismic waveforms and other geophysical parameters, we have embarked on a simultaneous, joint inversion of disparate data types to obtain models that benefit from the comparative strengths of the different parameters and can provide improved constraint where a single data type may be lacking. We have jointly inverted Bouger gravity observations, surface-wave dispersion curves and receiver functions to obtain a self-consistent 3D shear velocity/density model with improved resolution for shallow geologic structures. Jointly inverting these datasets with seismic body wave (S) travel times provides additional constraints on the shallow structure and an enhanced 3D shear wave model for our study area in western China.

Report Documentation Page

Form Approved
OMB No. 0704-0188

Public reporting burden for the collection of information is estimated to average 1 hour per response, including the time for reviewing instructions, searching existing data sources, gathering and maintaining the data needed, and completing and reviewing the collection of information. Send comments regarding this burden estimate or any other aspect of this collection of information, including suggestions for reducing this burden, to Washington Headquarters Services, Directorate for Information Operations and Reports, 1215 Jefferson Davis Highway, Suite 1204, Arlington VA 22202-4302. Respondents should be aware that notwithstanding any other provision of law, no person shall be subject to a penalty for failing to comply with a collection of information if it does not display a currently valid OMB control number.

1. REPORT DATE	2. REPORT TYPE	3. DATES COVERED
SEP 2008		**00-00-2008 to 00-00-2008**

4. TITLE AND SUBTITLE	5a. CONTRACT NUMBER
Geophysical Modeling in Eurasia: 2D Crustal P and LG Propagation; Upper Mantle Shear Wave Propagation and Anisotropy; and 3D, Joint, Simultaneous Inversions	5b. GRANT NUMBER
	5c. PROGRAM ELEMENT NUMBER
6. AUTHOR(S)	5d. PROJECT NUMBER
	5e. TASK NUMBER
	5f. WORK UNIT NUMBER
7. PERFORMING ORGANIZATION NAME(S) AND ADDRESS(ES) **Los Alamos National Laboratory,P.O. Box 1663 ,Los Alamos,NM,87545**	8. PERFORMING ORGANIZATION REPORT NUMBER
9. SPONSORING/MONITORING AGENCY NAME(S) AND ADDRESS(ES)	10. SPONSOR/MONITOR'S ACRONYM(S)
	11. SPONSOR/MONITOR'S REPORT NUMBER(S)

12. DISTRIBUTION/AVAILABILITY STATEMENT
Approved for public release; distribution unlimited

13. SUPPLEMENTARY NOTES
Proceedings of the 30th Monitoring Research Review: Ground-Based Nuclear Explosion? Monitoring?Technologies, 23-25 Sep 2008, Portsmouth, VA sponsored by the National Nuclear Security Administration (NNSA) and the Air Force Research Laboratory (AFRL)

14. ABSTRACT
see report

15. SUBJECT TERMS

16. SECURITY CLASSIFICATION OF:			17. LIMITATION OF ABSTRACT	18. NUMBER OF PAGES	19a. NAME OF RESPONSIBLE PERSON
a. REPORT **unclassified**	b. ABSTRACT **unclassified**	c. THIS PAGE **unclassified**	**Same as Report (SAR)**	**10**	

OBJECTIVES

The goal of our work is to develop geophysical models that improve the seismic phase travel-time predictions over the models currently used. Several different seismic phases are used in routine event location, and the models we currently employ require significant travel-time corrections for accurate arrival prediction; these corrections are spatially varying and different for different phases. We aim to develop models and methods whose ability to predict travel times can significantly reduce the magnitude of empirical corrections needed for accurate event location.

RESEARCH ACCOMPLISHED

We present progress to date for three distinct seismic modeling thrusts: (1) Pg (crustal, direct P-wave) phase propagation and Lg (crustal, shear body wave) phase propagation, (2) Sn (upper-mantle shear body wave) propagation, and (3) ongoing work towards joint, simultaneous inversion of Rayleigh (surface wave) group velocities, teleseismic P-wave receiver functions and Bouger gravity data from satellite observations, to determine 3D lithospheric shear-wave velocities. For Pg, Lg, and Sn, we are developing the models as two-dimensional (2D) velocity maps that can predict phase arrivals for any great circle path within the modeled region (e.g., Myers et al., this volume), with the addition of site corrections that are solved for simultaneously as we invert data for each of the phases modeled.

Pg and Lg Modeling

The Pg phase is a compressional body wave that travels within the Earth's crust and is reported at local-to-regional distances in many seismic catalogs. The Lg phase is the analogous crustal shear wave. We use catalog arrivals from the Los Alamos National Laboratory (LANL) Ground-Based Nuclear Explosion Monitoring Research and Development (GNEMRD) seismic database to develop a 2D Pg model and a 2D Lg model for Eurasia. About 10% of the events in this database are classified as having epicentral uncertainty known to within 25 km of the true location (GT 25 km, GT25; e.g., Bondár). A time-distance plot (Figure 1) for Pg and Lg arrivals in our database shows contamination due to phase misidentification, data-entry typographical errors resulting in 60 s offsets, and bad arrival-time picks for both phase types.

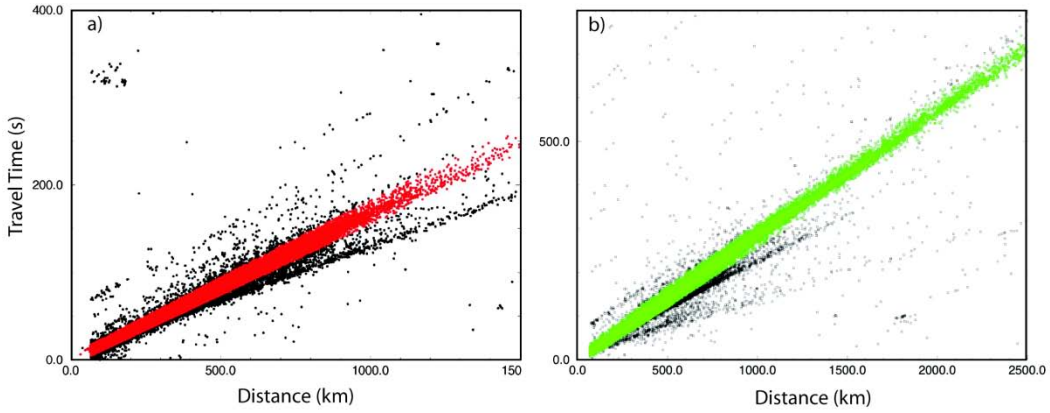

Figure 1. Time-distance plot showing phase arrivals in the LANL seismic database. (a) full dataset, which exihibits contamination from 60-s data-entry errors, poor phase picks, and misidentified Pn phase. Red dots indicate arrivals used in our Pg tomographic inversion. (b) Lg arrivals for the same GT25 events. Black dots show all arrivals, including 60-s data-entry errors, poor picks and misidentified Sn arrivals; green dots show arrivals used in our Lg tomographic inversion. From Steck et al., 2008.

For the Pg inversion, we have used 1,453,318 arrivals from 407,131 events recorded at 3,709 stations throughout Eurasia. For Lg, we use 1,049,125 arrivals from 266,751 events recorded at 3,084 stations (Steck et al., 2008). Data coverage is shown in Figure 2. To invert these datasets, we use a method analogous to Pn tomography, assuming a great circle path between source and receiver. Events used have depths of 33 km or less. Only path lengths between

0.5 and 14 degrees were used for Pg; path lengths of 0.7 to 25 degrees were used for Lg. In addition to solving for slowness along the great circle path, we also solve for both an event term and a site term to accommodate depth uncertainty and
near-receiver velocity effects, respectively. Site terms are damped so that they sum to zero. We use first-difference regularization over a 1×1 degree grid, and solve for slownesses using the LSQR conjugate gradient method (Paige and Saunders, 1982). We solve for slowness over a region from 0 to 89 degrees North latitude and –20 to 195 degrees East longitude.

We used checkerboard tests to test the ability of our data to resolve the study area. We examined checkerboard velocity anomalies using the available ray paths for 2-, 4-, and 10-degree squares with alternating velocity perturbations of +/-10%. Good resolution coverage is better for Lg than for Pg due to longer raypaths of Lg phases. The results of these resolution tests for both Pg and Lg are shown in Figure 3.

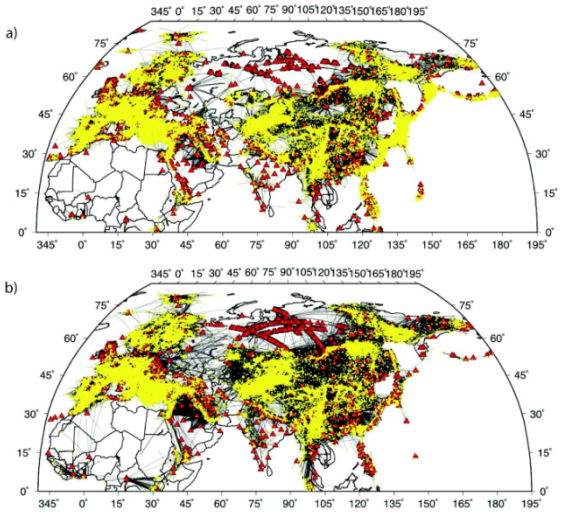

Figure 2. Ray diagram showing data coverage for Pg (2a) and Lg (2b). Yellow dots indicate events, and red triangles are receiver locations. Black lines indicate great circle paths used in the tomography. From Steck et al., 2008.

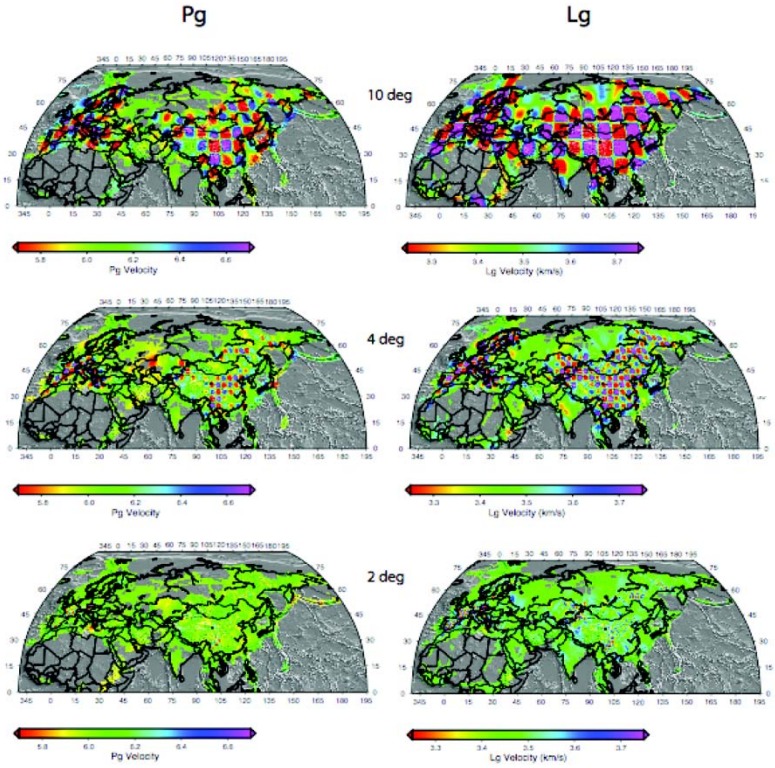

Figure 3. Checkerboard Pg and Lg resolution tests for 2-, 4-, and 10-degree velocity perturbation grids. From Steck et al., 2008.

For Lg, resolution is good throughout most of China and Mongolia as well as part of northeastern Russia and Kazakhstan. Europe, and Scandinavia are likewise well resolved. We also have some limited resolution for the Middle East and western India. Pg, on the other hand, has poorer resolution in all regions. At 2 degrees, only dense raypath regions are well resolved, including Western Europe and southcentral China.

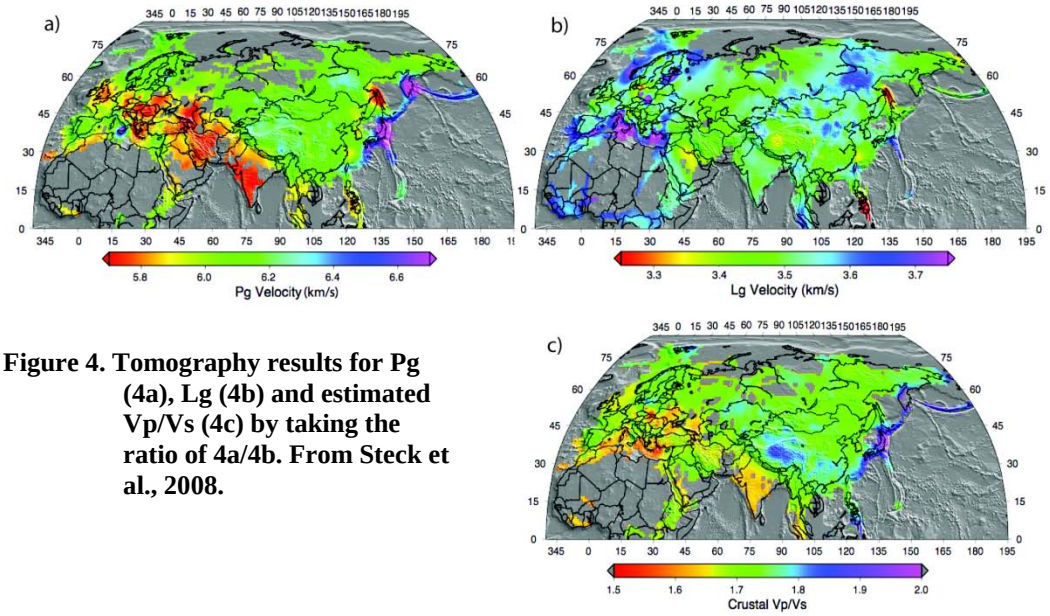

Figure 4. Tomography results for Pg (4a), Lg (4b) and estimated Vp/Vs (4c) by taking the ratio of 4a/4b. From Steck et al., 2008.

We show the inversion results in Figure 4. Pg appears fast in regions of convergence, such as the Pacific Rim. Most of Asia, from 80 degrees East to the continental margin, appears fast. The Middle East, India, Pakisan, and Kyrgystan appear slow, as do the Caspian Sea region and lower Volga. Scandinavia is average to fast, while most of Europe appears slow, except for Sicily, Spain, and central Turkey. Lg shows the bulk of Eurasia to be faster than average, with lower velocities manifested in parts of the Middle East, Gulf of Oman, Eastern Europe, central and northcentral Russia, Sakhalin Island, and Tibet. Vp/Vs ratios, computed by taking the ratio of the two tomographic maps, range from 1.7 near the Dead Sea to 1.9 in parts of Japan.

Sn Velocity

Following the technique of Phillips et al. (2007) that expanded on the Pn gradient method of Zhao (1993) and Zhao and Xie (1993), we have extended the Pn and upper-mantle Pn gradient tomography method to examine Sn and the upper-mantle Sn gradient for Eurasia. In our formulation, we will solve for great circle path Sn velocities as well as gradient and anisotropy, with static station and event correction terms (Begnaud et al., 2008). We depart from Phillips et al. by solving the gradient term in a nonlinear fashion, requiring an iterative approach. Our data consist of events that are GT25 and better. Sn arrivals from various global, regional, and local catalogs were merged (Begnaud et al., 2006). A vast majority of these data came from the ISC, ABCE (Lee et al., 2002), and Earthquake Data Report (EDR) of the National Earthquake Information Center (NEIC). We chose only events whose hypocentral depths are 50 km or less, and only arrivals having paths between 2.5 and 18 degrees were used; following culling of the data, which included a cursory 15-s residual trim relative to iasp91 and regularization with residual cutoffs, and limiting data range from 400 to 1700 km path lengths, our final data set consisted of 144,933 arrivals from 14,645 events recorded at 2,399 stations after discarding stations recording fewer than 10 events and events with fewer than 5 arrivals. Raypaths for our inversion are shown in Figure 5, indicating regions where we have good data coverage.

Our model was discretized in a 1-degree grid. Crustal thickness effects were estimated assuming 45-km average thickness, 3.6 km/s shear velocity, and a 52-degree incidence angle at both source and receiver. The event leg of the parameterization assumes the ray extends from the event depth to 45 km. We assumed a 4.55-km/s starting mantle velocity and 0.001/s starting mantle gradient. We regularized in both slowness and gradient using first differences. Damping from starting values used 30% of the smoothing value. We solved using the LSQR conjugate gradient approach (Paige and Saunders, 1982). Iterations continued until travel-time RMS change was less than 0.1 s; this was achieved in two iterations.

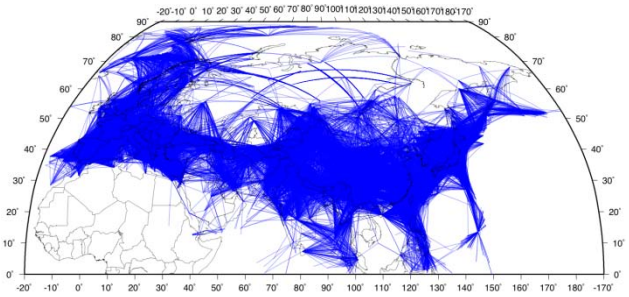

Figure 5. Raypath coverage for Sn tomography. From Begnaud et al., 2008.

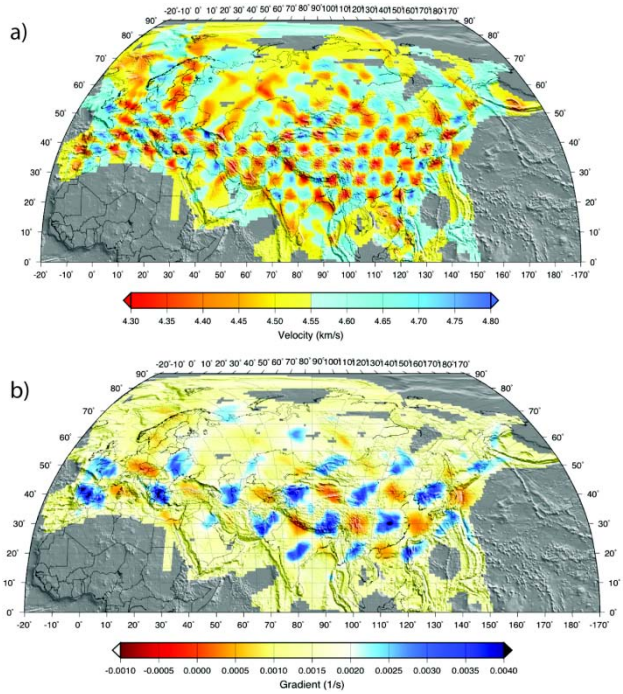

Figure 6. Results of checkerboard tests for Sn velocity (6a) and upper-mantle shear velocity gradient (6b). From Begnaud et al., 2008.

A further test of the data's resolving power was performed via the use of checkerboard velocity perturbations and velocity gradient perturbations. For the raypaths shown in Figure 5, we show the results of checkerboard tests in Figure 6. Upper-mantle S velocities were tested in 5-degree velocity cells using a 0.25 km/s anomaly from the starting model of 4.55 km/s, with 2.5 km/s Gaussian noise added. Resolution is good for much of Eurasia, although the Arabian Shield and Arctic are less well recovered. The upper velocity gradient was tested for 10-degree cells having 0.002/s perturbations from the starting value of .0015/s, with Gaussian noise of RMS 2.5 s added. The region showing resolution for gradient is roughly the same as for the Sn velocities.

Inversion results (Figure 7) show that Sn velocities generally exhibit the same patterns seen in Pn (e.g., Phillips et al., 2007), following expected variations for stable vs. tectonically active areas. The Sn gradient (Figure 7) is generally very low and even suggests negative gradients in areas such as eastern China and the Mediterranean, whereas it is relatively high in subduction zones and convergent plate margins (Tibet, Japan, and Korea) (Begnaud et al., 2008).

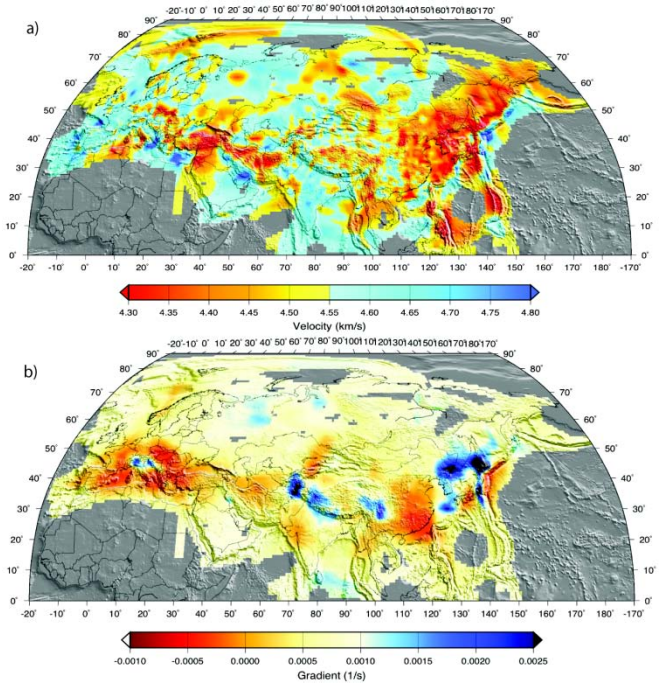

Figure 7. Sn velocities (7a) and velocity gradient (7b) found in our study. The values depicted here result from solving without including an anisotropy term. Data-fit improvement following inversion was 56%. From Begnaud et al., 2008.

When solving for upper-mantle gradient, the velocity seems to inversely adjust relative to gradient compared with solutions for velocity only (high gradients drive lower lid velocities). With few exceptions, station delays (Figure 8) follow known crustal thickness, with greater delays following mountain belts (the Himalayas, the Alps, the Appenines) and thicker lithosphere in platforms (Tibet, western China), while negative values are seen in areas of thinner lithosphere such as the Rhinegraben, east China, and the Mediterranean.

Figure 8: Station delays. From Begnaud et al., 2008.

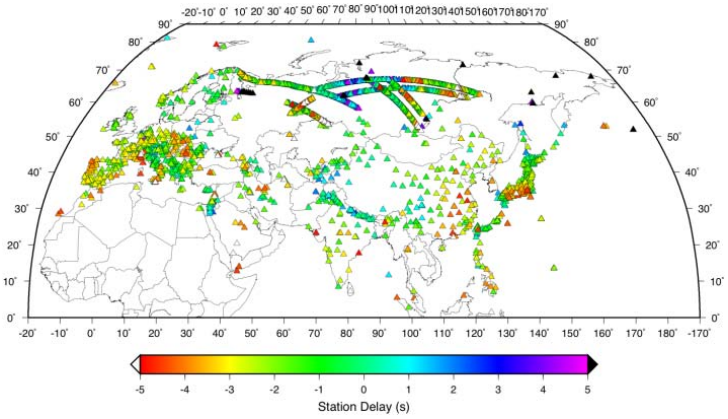

Solving for Sn anisotropy removes some of the high-frequency patterns in the Sn velocity. The anisotropy patterns we see follow those found by Pei et al. (2007) for Pn anisotropy in their study of China. Figure 9 illustrates a closeup view of China-East Asia Sn anisotropy obtained in our study.

Joint, Simultaneous 3D Tomography for Multiple Geophysical Datasets

It is well known that derivation of geophysical models for a given observable, such as body wave models or surface wave models, may provide good predictors of behavior for the specific parameter modeled but often provides poor prediction for other parameters, even when we have empirical or theoretical knowledge of how the parameters relate to one another. Due to the nonunique properties of inversion methods, we may often find a solution for one data type, but we must acknowledge that, although it can predict behavior of that data type, the solution is ambiguous and other models may serve equally well.

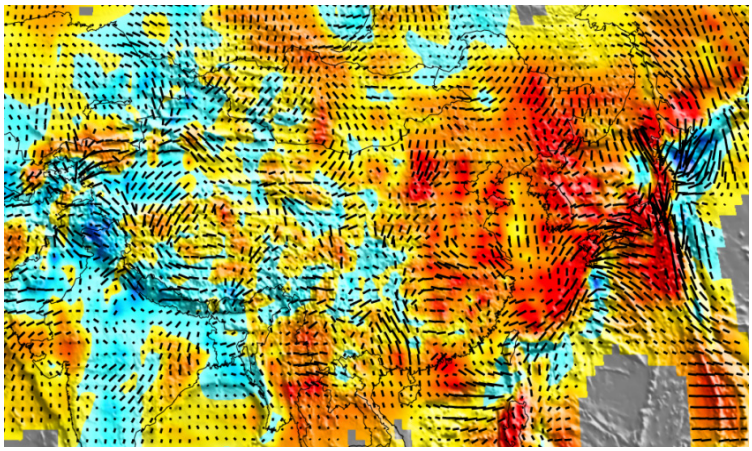

Figure 9. Sn anisotropy. Black lines indicate direction and relative magnitude of the fast direction. Note the apparent signal parallel to the Songpan Ganzi fold belt and the strong signal parallel to the Japanese and Phillippine subduction zones. Anisotropy appears weak in the Indian craton, Bay of Bengal, and the stable Shanxi Plateau. From Begnaud et al., 2008.

The materials whose properties we are modeling will influence not only the parameter in question but will also, at the same time, influence other geophysical parameters that we might also measure. Thus, a joint, simultaneous inversion of all pertinent and available data types for a region may provide us with a far more robust model than can be obtained by using only a single parameter. Moreover, the extent of our well-resolved model may be significantly expanded due to the variable coverage provided by different measurements, and its features may be better constrained due to the different resolving powers of different data types. For instance, it is becoming commonplace to derive seismic velocity models by jointly inverting surface wave dispersion values, which have the benefit of large regions of coverage but provide relatively little vertical control on impedance contrast interfaces, with seismic receiver functions, which by their nature are only point samples at the locations of seismic stations but which can provide detailed information about acoustic impedance interfaces at depth. The receiver functions by themselves are ambiguous in the depth-to-interface information, requiring some sort of a priori assumption of seismic velocities, but the surface wave modeling provides average velocities. These complementary characteristics can give us much greater confidence in the resulting inversion product. Inclusion of gravity data in the inversion provides increased resolution of shallow structures that are essentially invisible to the surface waves.

We have undertaken the 3D modeling of the Tarim Basin region using simultaneous joint inversion of surface wave dispersion (Maceira et al., 2005), teleseismic P-wave receiver functions (Ammon et al., 2004) and satellite gravity data obtained during the Gravity Recovery And Climate Experiment (GRACE) mission (Tapley, 2005). Recent adjustments to the inversion approach (Maceira and Ammon, 2008) include the use of Bouger gravity anomalies, as opposed to the free-air anomaly. This advance has proven to improve our resolution of the shallow structure, as topographic information is not included in the Bouger values. To invert for shear-wave velocities using the gravity data, we employ two empirical relationships to relate seismic velocity and density: for sedimentary rocks, the relationship developed by Nafe and Drake (1963) and for basement, Birch's Law (1961). A recent work by Brocher (2005) was tested (Maceira and Ammon, 2008) and found to provide no improvement to the fit for the GRACE gravity data for this region; clearly, additional work is warranted.

We parameterize the model as 1×1 degree boxes arranged in depth columns. Shear wave velocity values are treated as one-dimensional (1D) depth-dependent velocity profiles at the center of each cell, where we conisder fundamental mode group velocities and Bouger gravity anomalies computed against a background density model. Because the gravity values for any given cell are influenced by the surrounding cells, the model inversion uses a weighted factor of the values in neighboring cells, which we have determined is significant to three cell distances. We show the model parameterization in Figure 10.

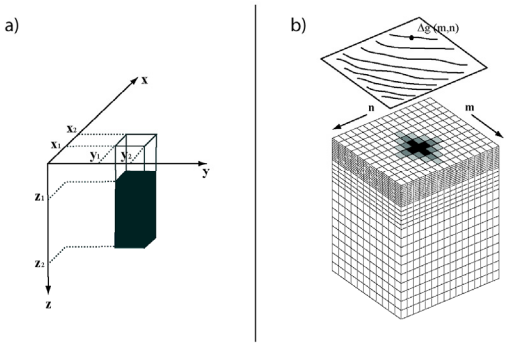

Figure 10. Model parameterization. Each 1x1 degree cell is a column characterized by a stack of density prisms and a suite of 1D fundamental mode group velocities. (a) A single cell with its input geographic coordinate system. (b) For a given cell (black), the influence on the gravity value will include densities of surrounding cells. Weighting of these cells decreases with distance, as suggested by changes in their gray shading (from Maceira and Ammon, 2008).

The new, jointly derived model can be best validated by showing improvements to predictions of independent data, which were not used in the development of the model. We have shown in previous presentations that the joint model provides a good simultaneous fit to the datasets used and that it agrees well with features known within the region studied. Our model requires slower velocities in the sedimentary basins than suggested by inversion of the surface wave data alone; this requirement is borne out through a comparison of waveform predictions using models derived from surface waves alone compared with the model derived in our joint inversion. Our test is focused on short periods, as these are the most influenced by shallow structure; moreover, improved fitting at short periods is needed if the monitoring community wishes to obtain reliable detections at lower thresholds (Taylor and Patton, 2006).

We demonstrate the method of Maceira (2006) applied to waveforms from 26 nuclear explosions. Displacement waveforms are passband filtered with center frequencies at 7, 10, 12, 16, and 20 seconds. Each bandpassed trace provided a particle motion window by multiplying the envelopes of the vertical and radial components, and a group velocity window, computed using minimum and maximum slowness values for the frequency of interest, calculated through both the joint 3D model and that derived solely from dispersion values. The measurement window is defined as the intersection of these two time windows. Amplitudes are measured only for the portion of the waveform found within the measurement window. If the particle motion and arrival time windows do not intersect, no measurement is possible.

We illustrate the results of both cases in Figure 11.

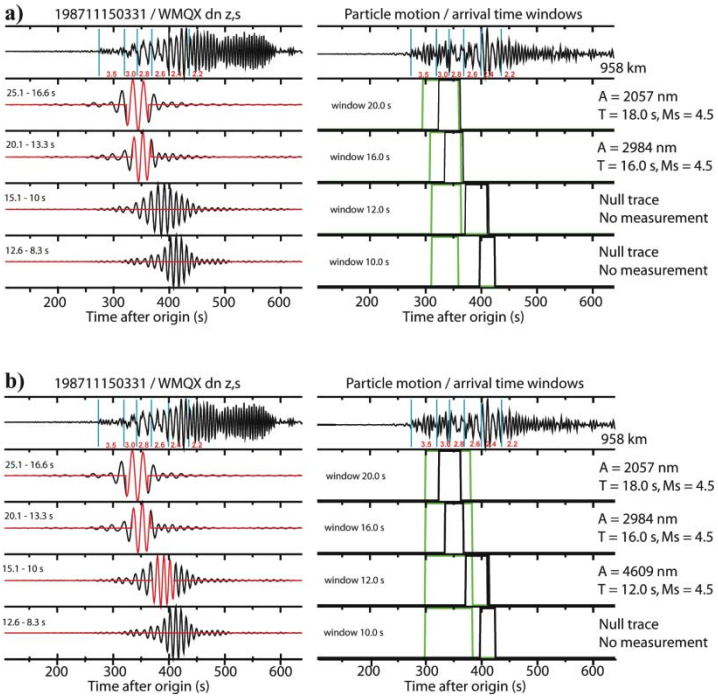

Figure 11. Surface wave prediction comparing use of dispersion data (11a) with results using the combined datasets in joint inversion. Waveform matching is successful over shorter periods for predictions of the joint inversion (11b, left panel) compared with inversion from surface wave data alone (11a, left panel) due to better overlap of the group velocity window and particle motion window (green and black windowed boxes, respectively) for joint inversion (11b, right panel) compared with surface wave dispersion data alone (11a, right panel). From Maceira and Ammon, 2008.

Calculations used from the joint 3D model were better able to predict the arrival of surface waves at short periods (compare the windows at 12 seconds). We found that in 73% of the cases the joint inversion 3D model was better able to predict surface wave arrivals at short periods than the model derived from dispersions alone.

Our method is being further refined through the addition of body wave travel-time data (S-wave arrivals) into the joint, simultaneous tomographic inversion. We begin by testing the method on a small piece of the test region; a time-distance plot for S-wave arrivals for the small study area is shown in Figure 12. Inclusion of these body wave travel times does not aid in resolution of deeper structure, as raypaths are limited to the crust and uppermost mantle; however, in the shallow part of the model, including the sedimentary basins, these data can significantly aid in resolution of more-detailed structure. Ray coverage for these data is shown in Figure 13. Although for the most part, these fine details will have little influence on longer-period surface wave modeling, we expect them to improve our capabilities at shorter periods, which are crucial for lower-magnitude threshold requirements.

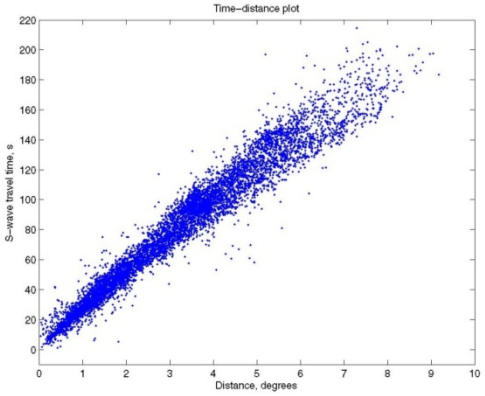

Figure 12. Time-distance plot for S-wave arrivals used in preliminary test of joint inversion method with body-wave travel-time data. Although some scatter can be seen, in general, the well-behaved data should enhance resolution of shallow (crustal) structure in our inversion.

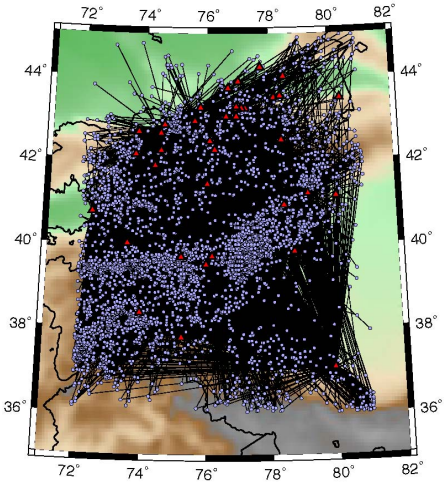

Figure 13. S-wave raypaths integrated into a joint inversion test study. Red triangles represent seismic stations, and the blue dots are sources. This small pilot study images only the western half of the Tarim Basin.

CONCLUSIONS AND RECOMMENDATIONS

We continue to explore the various data types important to robust characterization of the Earth for seismic monitoring. Pg and Lg tomography leads to better understanding of the crustal influence on seismic travel times; crustal effects are increasingly important as we move toward near-regional and local monitoring. Because the increasing use of secondary phases is expected to become important in precise event location, we need data-driven models wherever possible to correctly predict travel times for these phases. The Sn tomographic analysis is likewise important for the use of Sn arrivals in location and to enhance our understanding between the well-studied Pn characteristics of Eurasia and the relationship with the Sn phases. Travel-time prediction may depend also on our correct accounting for travel-time anisotropy, which has been only superficially addressed for Pn and not examined by many researchers for Sn, due largely to the comparative lack of data for this phase. We have demonstrated a significant improvement in prediction capability of our 3D models when joint, simultaneous inversion of multiple datasets is performed. Increased resolution of shallow structures and sedimentary basins, arising from the inclusion of such parameters as Bouger gravity anomalies and/or seismic body wave arrival times, can aid us in our prediction of surface wave dispersion at shorter periods, which is essential to lowering the magnitudes at which our predictions are dependable.

ACKNOWLEDGEMENTS

D. F. Baker and M. Romero-Yeske performed data analysis, providing parameters used in these models. J. A. Chang and R. Stead provided important database support, without which these studies would not be possible. Our thanks to J. Benson and M. Wetovsky for editorial assistance.

REFERENCES

Ammon, C. J., W. Sevilla, R. B. Herrmann, and G. E. Randall (2004). Systematic inversion of receiver functions and surface wave dispersion for crustal structure in central Asia, in *Proceedings of the 26th Seismic Research Review: Trends in Nuclear Explosion Monitoring*, LA-UR 04-5801, Vol. 1, pp. 29–38.

Begnaud, M. L., L. K. Steck, and C. A. Rowe (2006). Improving seismic event locations in Asia by using catalog-scale empirical travel time correction surfaces, *EOS Trans. AGU* 87 (52), Fall Meet. Suppl., Abstract T51D-1550.

Begnaud, M. L., W. S. Phillips, C. A. Rowe, and L. K. Steck (2008). Sn velocity, gradient and anisotropic variations in the upper mantle of Eurasia (abstract), *Seismol. Res. Lett*. 79: 345.

Birch, F. (1961), The velocity of compressional waves in rocks to 10 kilobars, part 2, *J. Geophys. Res.* 66: 2199–2224.

Bondár, I., S. C. Myers, E. R. Engdahl, and E. A. Bergman (2004). Epicentre accuracy based on seismic network criteria, *Geophys. J. Int.* 156: 483–496.

Lee, W. H. K., H. Kanamori, P. C. Jennings, and C. Kissling (Eds.) (2002). *International Handbook of Earthquake and Engineering Seismology* (CD-ROM), Elsevier, New York.

Maceira, M. and C. J. Ammon (2008). Joint inversion of surface wave velocity and gravity observations and its application to Central Asian basins shear velocity structure, *J. Geophys. Res*. (in press).

Maceira, M. (2006). Surface waves, Earth structure, and seismic discrimination, Ph.D. thesis, Pennsylvania State University, State College, PA.

Maceira, M., S. R. Taylor, C. J. Ammon, X. Yang, and A. A. Velasco (2005). High-resolution Rayleigh wave slowness tomography of central Asia, *J. Geophys. Res*. 110: B06304, doi:10.1029/2004JB003429.

Nafe, J. E. and C. L. Drake (1963). *Physical Properties of Marine Sediments, in The Sea*, Vol. 3, M. N. Hill (Ed.). New York: Interscience, pp. 794-815,

Pei, S., J. Zhao, Y. Sun, Z. Xu, S. Wang, H. Liu, C. A. Rowe, M. N. Toksöz, and X. Gao (2007). Upper mantle seismic velocities and anisotropy in China determined through Pn and Sn tomography, *J. Geophys. Res*. 112: B05312, doi:10.1029/2006JB004409.

Phillips, W. S., M. L. Begnaud, C. A. Rowe, L. K. Steck, S. C. Myers, M. Pasyanos, and S. Ballard (2007). Accounting for lateral variations of the upper mantle gradient in Pn tomography studies, *Geophys. Res. Lett*. 34: L14312, doi:10.1029/2007GL029338, 2007.

Steck, L. K., W. S. Phillips, M. L. Begnaud, R. Stead, and C. A. Rowe (2008). Seismic tomography of Pg and Lg and its use for average upper crustal structure in Eurasia (abstract). *Seismol. Res. Lett*. 79: 305.

Tapley, B., J. Ries, S. Bettadpur, D. Chambers, M. Cheng, F. Condi, B. Gunter, Z. Kang, P. Nagel, R. Pastor, T. Pekker, S. Poole, and F. Wang (2005). GGM02 - An improved Earth gravity field model from GRACE, *J. Geodesy*, DOI 10.1007/s00190-005-0480-z.

Taylor, S. R. and H. J. Patton (2006). A probability of detection method for reducing short-period mb −Ms false alarm rates, *Bull. Seismol. Soc. Am*. 96: 1078–1090.

Zhao, L.-S. (1993). Lateral variations and azimuthal isotropy of Pn velocities beneath Basin and Range province, *J. Geophys. Res*. 98: B12: 22109-22122.

Zhao, L.-S. and J. Xie (1993). Lateral variations in compressional velocities beneath the Tibetan Plateau from Pn traveltime tomography, *Geophys. J. Int*. 115: 1070–1084.